

Marine heatwave events strengthen the intensity of tropical cyclones

Hwan-Young Choi^{1,2}, Myung-Sook Park^{id 2,3✉}, Hyeong-Seog Kim^{id 1,3✉} & Seonju Lee²

Marine heatwaves become more frequent and stronger due to global warming. It is necessary to clarify how and by which process marine heatwaves affect marine weather systems. Here, we examine how marine heatwaves strengthen tropical cyclones. We analyze 128 tropical cyclones that intensified with marine heatwaves and 184 tropical cyclones that intensified without marine heatwaves over the western North Pacific and Atlantic. Marine heatwaves finally lead to a maximum intensity of 35.4% stronger (106.72 kts) tropical cyclone. Notably, satellite data reveal that marine heatwaves are associated with precipitation-richer tropical cyclone conditions despite similar tropical cyclone intensities. Due to the increased latent heat flux during marine heatwaves, intensified precipitation near the tropical cyclone center contributes to the intensification process. This study provides insights into how more frequent marine heatwaves by global warming impact tropical cyclones.

¹Ocean Science and Technology School, Korea Maritime and Ocean University, Busan, Republic of Korea. ²Korea Ocean Satellite Center, Korea Institute of Ocean Science & Technology, Busan, Republic of Korea. ³These authors jointly supervised this work: Myung-Sook Park, Hyeong-Seog Kim. ✉email: mspark@kiost.ac.kr; hyeongseog@kmou.ac.kr

Marine heatwaves (MHWs), extreme ocean warming events that last from several days to weeks, have attracted social and scientific attention due to their devastating effects on marine ecosystems and economic impacts on fishery industries¹. In addition to ecological and social effects, MHWs with a warm ocean thermal structure^{2–4} can physically interact with atmospheric phenomena such as the El Niño–Southern Oscillation⁵, atmospheric heatwaves⁶, and tropical cyclones (TCs)⁷. As MHWs become more frequent and robust under global warming^{1,8,9}, it is crucial to understand how and by which process MHWs affect marine weather systems.

TCs last a few days to several weeks and are short-term marine weather events that can cause enormous social and economic damage. In general, previous studies^{10–12} using high-resolution global climate models have shown that in a warming climate, the frequency of TCs tends to decrease, but the frequency of intense TCs (Category 3 or higher-level) increases. Additionally, the TC-related precipitation rates increase as the moisture content in the atmosphere increases due to anthropogenic global warming^{13,14}. Nevertheless, previous investigations of the global warming impact on TCs have mainly focused on the annual means of TC activities and frequencies rather than the short-term TC evolution. Some of the previous studies^{15,16} also show the extremely high Sea Surface Temperature (SST) impact on TC intensity, but most were limited to a few TCs and specific cases only. Thus, in this study, we conducted a large-scale statistical analysis of interactions between an extremely warm environment and TC evolution on a time scale of several days during MHW.

Following previous studies^{17,18}, the warm ocean thermal structure induced by MHW events might be a favourable environment for TCs. When an MHW occurs, increased shortwave radiation due to the shallower mixed layer depth enhances warming and increases upper ocean stratification^{19,20}. Moreover, the strong stratification reduces vertical mixing and heat transport²¹. This structure elevates the upper ocean heat content and lifts warm anomalies from the subsurface. Recently, Dzwonkowski et al.⁷ showed that an MHW in the northern Gulf of Mexico developed due to an atmospheric heatwave and a preceding TC. This MHW event, with a high SST (>32 °C) and strong ocean stratification, supplied thermal energy and led to the intensification of Hurricane Michael (2018) to Category 5. Rathore et al.²² showed the interactions between an MHW and TC Amphan in the Bay of Bengal in 2020. The TC heat potential increased by anomalously high thermal stratification maintained the MHW and contributed to TC Amphan intensification.

These impacts of an MHW on a single TC case motivated the current comprehensive investigation of how MHWs affect multiple TCs. We analyzed 312 TCs that intensified over the western North Pacific (WNP) and the Atlantic (ATL) Oceans from 1982 to 2019. In this study, we mainly focus on the intensity change of the TC when the MHW event occurred before reaching the maximum TC intensity. Therefore, we examined the day-to-day evolution of TC intensification from 5 days before the lifetime maximum intensity (LMI) to 2 days after the LMI. By analyzing the convection and the air–sea interaction, we determined by which process the MHW events contribute to TC intensification. We analyzed the precipitation and surfaced latent heat flux near the TC center. The results show that TCs intensify more rapidly under the influence of MHWs via much larger latent heat flux from the ocean and precipitation-rich conditions to boost TC intensification.

Results

MHW impacts on TC intensity and intensification evolution. This study first examines the evolution of TC intensity between

MHW versus non-MHW TCs in Fig. 1a. Notably, significant distinctiveness exists in TC LMIs. The average LMI (106.72 knots) for the MHW TCs was 28 knots higher than that for the non-MHW TCs (78.80 knots). The apparent intensity difference began to appear on Day –3 (3 days before LMI), although MHW TCs were slightly weaker on Day –5. From Day –3 through LMI Day, the MHW TCs intensified more rapidly (12.52 knots day^{–1} on Day –2 and 17.32 knots day^{–1} on Day –1) than the non-MHW TCs, with 95% significance. The TC intensification rates for MHW TCs are about three times higher than those for non-MHW TCs: 4.5 vs. 12.5 knots day^{–1} on Day –2. The more substantial intensification of MHW TCs can also be seen in the proportion of TCs in the Saffir–Simpson Hurricane category (Fig. 1d). The ratio of Category 4 and Category 5 (called a super typhoon/hurricane) is 53.9% for MHW TC and 22.8% for non-MHW TC. The TCs that experienced MHWs are more than twice as likely to grow into super hurricanes/typhoons as they do not. The drastic strengthening of TCs that pass an MHW area is consistent with a case study by Dzwonkowski et al.⁷ or Rathore et al.²².

The TC intensity evolution in the WNP and ATL regions shows similar trends, although slight differences exist. In the WNP, the intensity difference between the MHW and non-MHW TCs is 4.8 knots on Day –2, 13.76 knots on Day –1, and 27.28 knots on LMI Day with 95% significance. In addition, the intensity difference for ATL is 13.45 knots on Day –2, 17.85 knots on Day –1, and 27.37 knots on LMI Day, which reveals larger intensity differences in the ATL than in the WNP. Nevertheless, the TC intensification rate for MHW TCs in the WNP (19.97 knots day^{–1}) is ~2.5 times more rapid than the ATL case (7.89 knots day^{–1}) on Day –1. As a result, the ratios of the super typhoon/hurricane for MHW TCs are 58% in the WNP and 39.3% in the ATL, while those for non-MHW TCs are 25.6% and 14.9%, respectively. Mean SST over the WNP warm pool area is climatologically higher than ATL, and the MHW intensity is also 0.2 °C higher in the WNP than ATL, which may result in a difference in TC intensity rate between WNP and ATL. The doubling in the chances of developing into a super typhoon/hurricane for MHW TCs occurs in both basins. It confirms that MHWs are favorable to strengthening TCs in both basins.

Precipitation evolution near the TC center. The characteristics and distribution of convection are closely related to TC intensity changes. Chang et al.²³ showed that the multiday evolution of convective bursts in weak wind shear conditions is critical during WNP tropical cyclone development. The convective bursts in the pre-TC had a lower tropospheric maximum in latent heat, which makes these conditions more advantageous for TC genesis and intensification^{24–26}. Within convection, convective hot towers processing cyclonic vorticity (vortical hot towers; VHT)^{27,28} affecting TC development and intensification²⁹ produce intense precipitation.

Figure 2 shows the evolution of TRMM TMPA precipitation from Day –5 to LMI Day within 5 degrees from the circulation center. The mean precipitation for MHW TCs within 5 degrees from TC center is ~1.5–2 times greater than that for non-MHW TCs. Notably, the precipitation for the MHW TC is much stronger from Day –5 to Day –4 despite the MHW TCs' intensities remaining similar to non-MHW TCs during that period (Fig. 1). Moreover, the mean MHW TC precipitation increases rapidly from Day –4 to Day –2 (75.47%; 5.3 mm hr^{–1} to 9.3 mm hr^{–1}) (Fig. 2 k). In non-MHW TCs, the precipitation continues to increase until reaching the LMI, but the precipitation is weaker.

In particular, the MHW TCs have extremely heavy precipitation (>10 mm hr^{–1}, red contours in Fig. 2h–j) concentrated

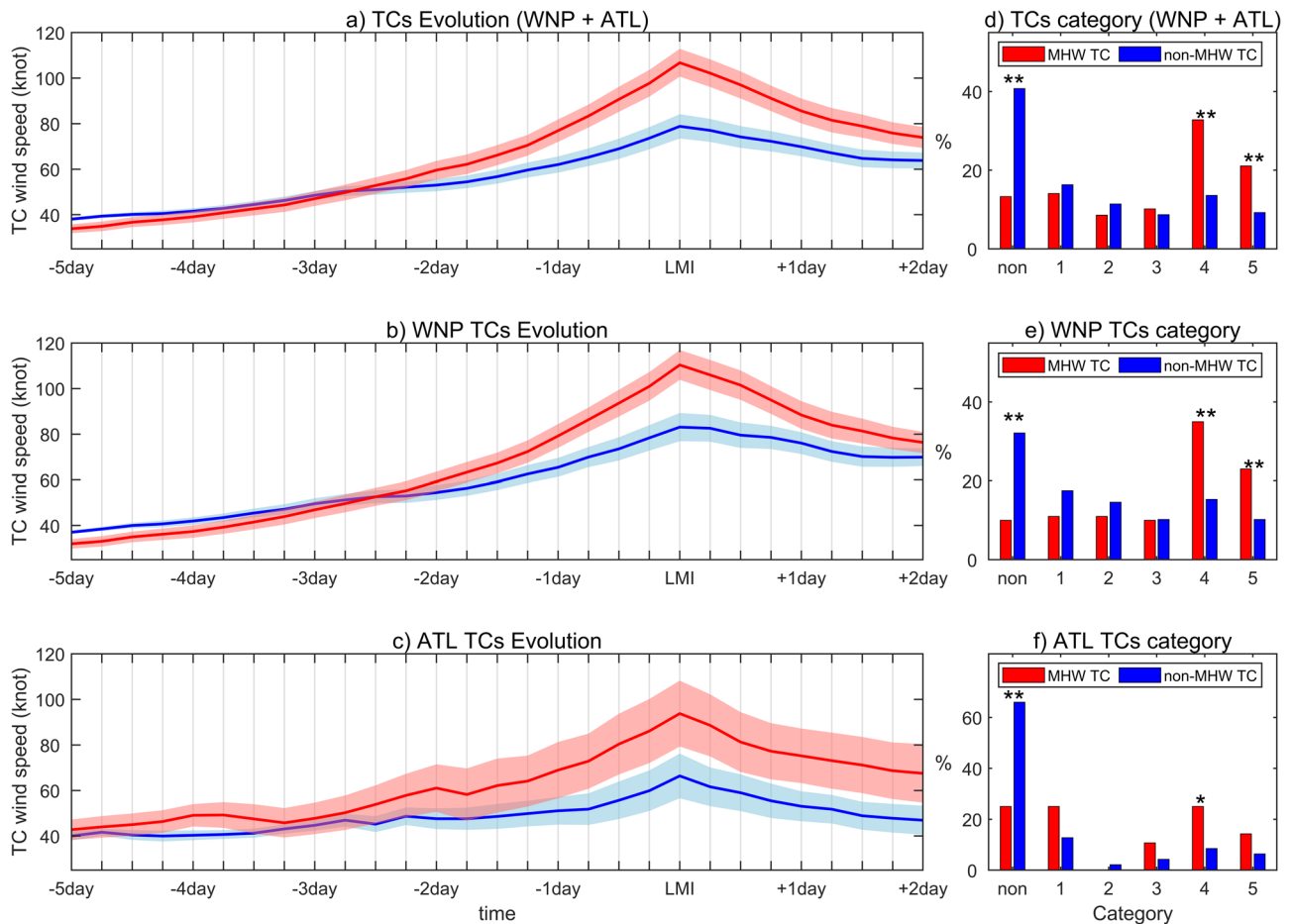


Fig. 1 TC evolution and category of MHW TC and non-MHW TC. **a–c** TC evolution of non-MHW TCs (blue line) and MHW TCs (red line) with different time steps based on LMI. The shading indicates the 95% confidence level value. **a** ALL (WNP + ATL) **b** for WNP region **c** ATL region. **d–f** Proportion of the Saffir-Simpson Hurricane categories for non-MHW TC (blue bar) and MHW TC (red bar). * and ** indicate that the difference between the two groups is statistically significant at the 90% and 99% confidence levels.

within a radius of 1–2 degrees from Day –3 to 0 Day. Without the MHW events, TCs do not reach such high precipitation near the center (Fig. 2a–e). The precipitation-rich conditions for MHW TCs may result from more vigorous convection at the ocean-atmosphere boundary. As in Molinari and Vollaro³⁰, the rapid deepening of Tropical Storm Gabrielle in 2001 is attributed to the development of the intense cell that enhanced diabatic heating close to the center in a region of high efficiency of kinetic energy production. In the MHW TCs, heavy precipitation near the storm center means that vigorous convection feeds off moisture convergence, and the release of LH near the center of the TC drives the overturning secondary circulation in the vital updraft region (Supplementary Figs. 1 and 2). In non-MHW conditions, such center-concentrated precipitation patterns remain unclear until Day –3, and only moderate precipitation (dashed line in Fig. 2c–e) evolved from Day –2. Overall, the impacts of the MHWs on TCs induce precipitation-rich conditions with the heavy precipitation peak (~convective cells) near the TC center, which may continue to lead to faster TC intensification. Such precipitation intensity and pattern during the MHW events may be attributed primarily to the favorable ocean environments.

How MHWs induce precipitation-rich TCs (air-sea interactions). To understand how warm subsurface ocean water layers during an MHW induce precipitation-rich TCs and subsequent TC intensification, we examine surface latent heat flux changes in

the interaction between the ocean and the atmosphere. Figure 3 shows the spatial distribution of the surface latent heat flux near the TC circulation center and the time series of the spatially averaged latent heat flux. In ECMWF, latent heat flux was calculated using the following equation:

$$J_q = -\rho C_Q |U_n| \left\{ \alpha_{surf} q_{sat}(T_{sk}) - \alpha_n q_n \right\} \quad (1)$$

where J_q is the surface humidity flux; ρ is the density; C_Q is the transfer coefficient for moisture; $|U_n|$ is the horizontal wind speed; α_n and α_{surf} are the updraft fraction at the lowest model level and at the surface; q_n is the specific humidity at the lowest model level; q_{sat} is the saturation specific humidity at the surface temperature T_{sk} ³¹. Following this equation, the surface latent heat flux (J_q) resulting from water phase changes, such as evaporation or condensation between the sea surface and the atmosphere through the effects of turbulent air motion.

Both non-MHW TC and MHW TC cases show negative-signed latent heat fluxes, indicating the latent heat supply from the ocean to the atmosphere. The latent heat flux for MHW TC is 1.8 to 3 times more than non-MHW TC throughout the TC intensifying period. The latent heat flux supply for MHW TCs increased broadly near the TC center from the early stage. In particular, the rate of release increases by 82.97% (–98.11 Wm^{–2} to –179.51 Wm^{–2}) from Day –4 to Day –2 (Fig. 3k). After Day –2, increasing latent heat fluxes are concentrated particularly within the eyewall surrounding the TC center (Fig. 3i, j). For the

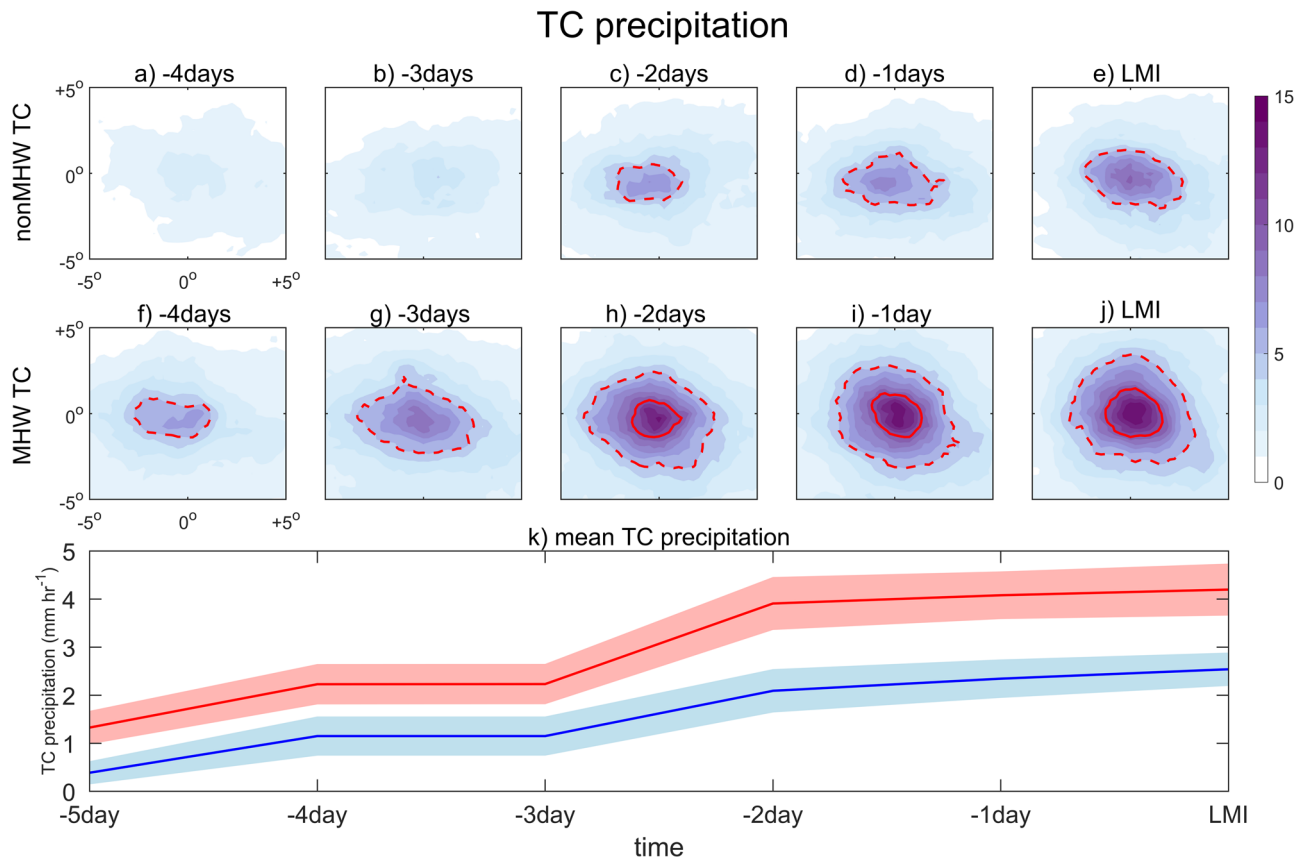


Fig. 2 TC precipitation changes in MHW TC and non-MHW TC. Composite mean precipitation (mm hr^{-1}) at relative times (Day -5 to Day 0) to the LMI Day. Precipitation was composited with a radius of 5 degrees based on the TC's center. **a–e** non-MHW TC and **f–j** MHW TC precipitation changes (shading, color bar at the right) with two precipitation intervals, 10 (5) mm hr^{-1} in red solid (dashed) line. **k** Time series of mean precipitation averaged over a circle within a radius of 5 degrees. The red line represents MHW TCs, and the blue line represents non-MHW TCs. The color shading shows a 95% confidence interval.

non-MHW TC case, the latent heat flux peak near the center was not apparent until Day -3 (Fig. 3c–e). Compared to that of MHW TCs (Fig. 3f–i), the development of non-MHW TCs is slower.

The latent heat supply from the ocean to the atmosphere can be attributed to two factors: higher surface wind speeds and/or moisture disequilibrium between the ocean surface and the atmosphere^{28,32}. Figure 4 shows the time series of the two main factors of latent heat flux: different specific humidity between the ocean surface and atmosphere ($q_{\text{sat}}(T_{\text{sk}}) - q_n$) and magnitude of surface wind speed ($|U_n|$).

The higher magnitude of latent heat fluxes for the MHW cases at the earlier phase (-5 Day to -3 Day) is dominated by the moisture disequilibrium (Fig. 4a) over the extremely high ocean temperature. During MHW event, the subsurface temperature is high, and the warming area is deeper and wider, resulting in high ocean heat contents (Supplementary Fig. 3). When a TC passes over a high ocean heat content area with MHWs, it can gain more latent heat flux from the ocean^{32,33} than a TC without such extreme ocean warming. In this process, the increased latent heat flux over the MHW TC region triggers more vigorous convection (Fig. 2) near the TC center by providing the energy needed for moisture to evaporate from the ocean surface and then condense in the atmosphere, which leads to precipitation-rich conditions (Fig. 2) and favors more drastic intensification (Fig. 1) in the following days. The increased latent heat flux pattern in rapidly intensifying TCs was seen in previous studies^{17,34–38}.

From Day -3 (TC intensity: MHW TCs > Non-MHW TC, Fig. 1), the surface wind speeds for MHW TC have overtaken

those for Non-MHW TCs (Fig. 4b). Once TCs become powerful, stronger TC-induced surface wind can extract more latent heat from the ocean to the atmosphere, especially near the TC center (Fig. 3i, j). This positive feedback in the air–sea interaction can further accelerate the TC intensification process. Accordingly, the TC intensification occurs more rapidly as approaches to LMI.

Discussion

In this research, we present evidence that TCs intensify more strongly and rapidly under the influence of MHW events. This study shows comprehensive analyses of the relationship between the MHW and TCs using multiple TCs over the WNP and ATL oceans (128 MHW TCs and 184 non-MHW TCs). We focus on the daily evolution of the TC intensity change from Day -5 Day to Day $+2$ relative to the TC maximum intensity day (Fig. 1). After passing the warm anomaly associated with MHW events, the averaged LMI of all MHW TCs (106.72 kts) is 27.92 knots higher than that of non-MHW TCs (78.80 kts), showing remarkable intensity discrepancies from Day -3 . Satellite investigation of precipitation evolution near the TC center was performed to understand the role of convection over the underlying warm ocean anomaly during MHW events (Fig. 2). Despite the similar TC intensities at the beginning, more vigorous convection in association with MHWs is evident near the TC center from Day -4 over the underlying warm ocean anomaly. In the air–sea interaction process, a much larger latent heat flux (Fig. 3) would

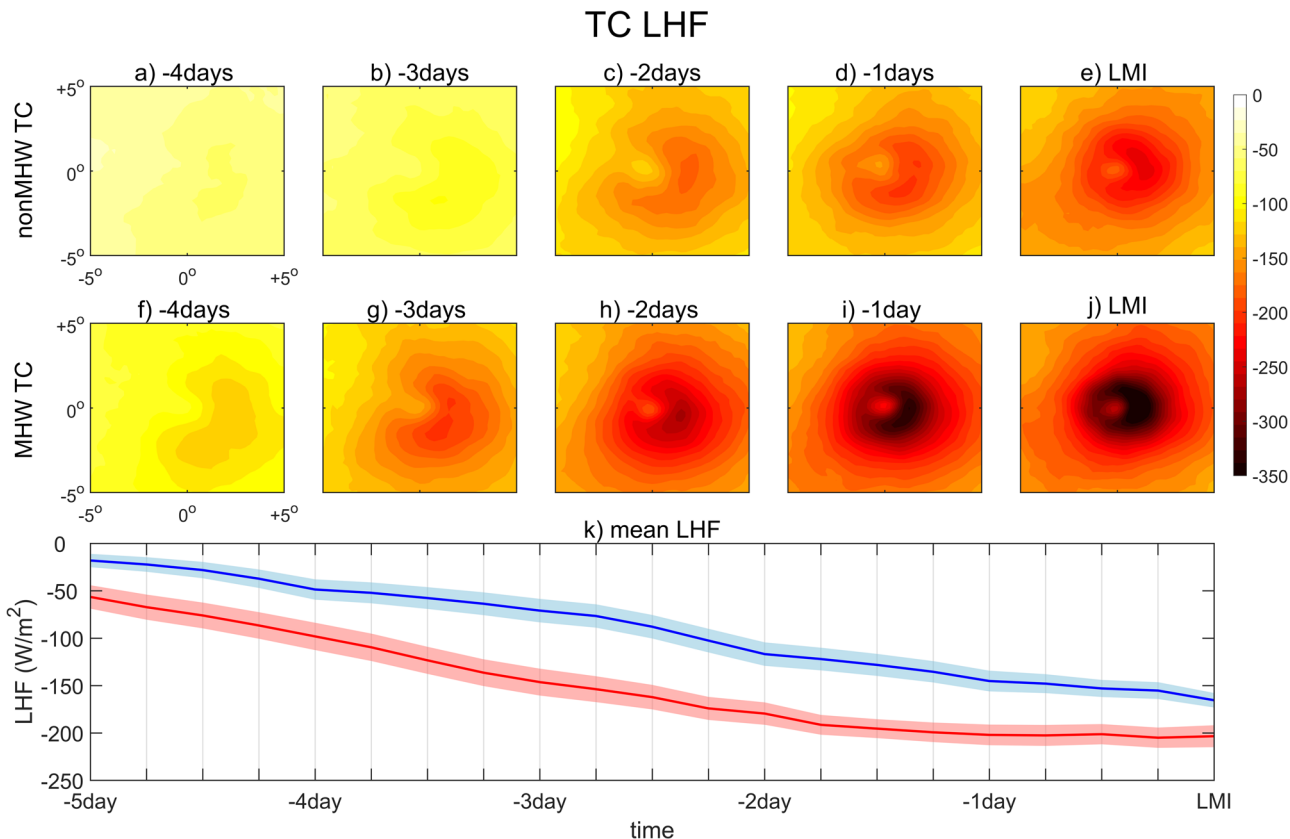


Fig. 3 TC Latent heat flux changes in MHW TC and non-MHW TC. **a-j** Composite mean latent heat flux at different times with respect to LMI Day and **k** spatially averaged latent heat flux for MHW TC (red) and non-MHW TC (blue) for 6-hour interval. The 95% confidence intervals are shaded with paint color.

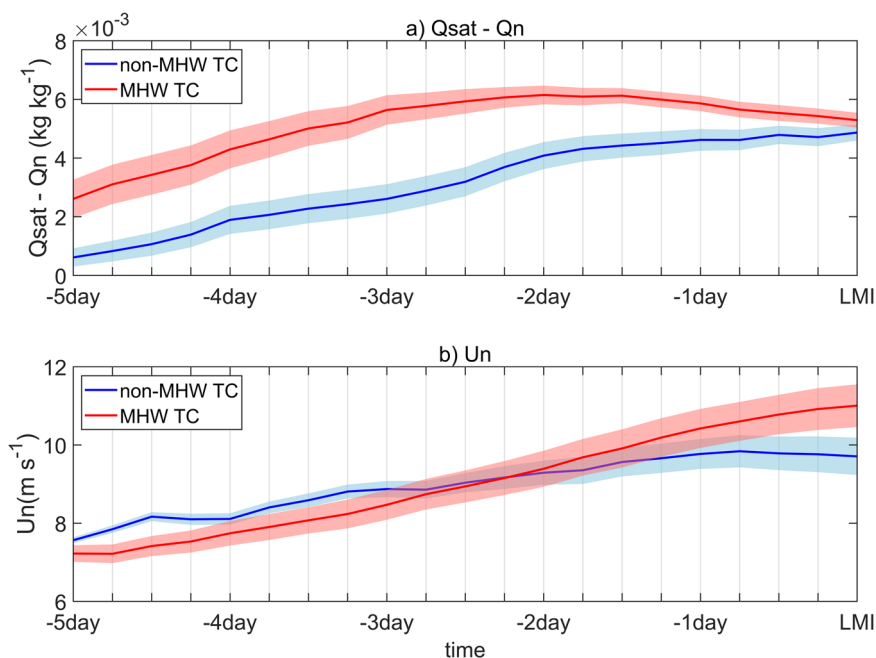


Fig. 4 TC Moisture disequilibrium and surface wind speed changes in MHW TC and non-MHW TC. Same as Fig. 3k, except for **a** the difference in the saturation specific humidity at the surface temperature (Q_{sat}) and specific humidity at the lowest atmosphere level (Q_n), and **b** the magnitude of surface wind speed (U_n). The 95% confidence intervals are shaded with paint color.

fuel the continuous convection process and promote heavy precipitation. Without an MHW event, the latent heat flux tends to be low, which is less favorable to heavy rainfall near the TC center and subsequent TC intensification. Increasing water vapor in the atmosphere due to the warm ocean anomaly during MHW events is favorable for initiating convective updraft regions, which would be expected to lead to a VHT in a vorticity-rich environment^{24,39,40}. The aggregation and merging of VHTs into system-scale circulation can cause intense TCs^{28,40}.

We also investigate whether favorable atmospheric conditions under the marine heatwaves can boost TC intensification. The vertical wind shear, one of the atmospheric dynamic conditions affecting TC intensification, was not critical for TC intensification for the MHW TCs. That is, the large-scale vertical wind shear magnitudes during the MHW TCs were about $1.4\text{--}4.7\text{ ms}^{-1}$ larger than those during non-MHW TCs, which rather inhibiting TC intensification^{22,39–41} (Supplementary Fig. 4a). By contrast, the atmospheric thermodynamic conditions (e.g., moisture convergence and mid-level relative humidity) for the MHW TCs are more favorable to intensify TCs, which are physically reasonable given higher SST condition (Supplementary Fig. 1 and Fig. 4b). Over higher SST anomaly region during the MHWs, moisture disequilibrium between air and sea (with more significant latent heat fluxes) may provide more water vapor contents in lower atmosphere, which induce more robust moisture convergence and mid-level humidity. These favorable thermodynamic atmospheric conditions during the MHWs are fundamentally connected to a precipitation-rich environment, leading to a more efficient TC intensification process.

Accordingly, this study highlights the critical role of MHWs in intensifying TCs by providing more latent heat flux from the ocean and heavier precipitation near the TC center. At the early stage of the MHW TC intensification process, the moisture disequilibrium plays a more critical role in the latent heat supply from the warm ocean to the atmosphere. Also, as TC with the MHW strengthens, the TC-induced stronger surface wind speed induces more latent heat supply from the sea. In this positive feedback, TC can rapidly intensify up to the LMI. This study establishes the physical connection between MHW events and TC intensity. Until now, the global warming impacts on TCs have

been understood mainly through changes in the annual TC intensity^{10–12}. Recently, CMIP6 model simulations⁴² have shown that MHWs will become more frequent and last longer under global warming. Thus, the current comparison framework between MHW TCs and non-MHW TCs will provide new insights into how global warming will alter the short-term TC evolution mechanism. The current study shows the physical impact of MHW events on the intensity of TC, which is one of the extreme weather systems, implying an overall physical influence on other marine weather systems interacting with the ocean, such as tropical mesoscale convective systems and rainfalls over the ocean⁴³.

Methods

Data. This study includes analyses of TCs over the WNP and the ATL from May to October (MJJASO) of 1982–2019. The TC position and intensity were obtained from the Joint Typhoon Warning Center (JTWC) Best Track data and the hurricane database (HURDAT2) for the WNP and ATL, respectively. In this study, the formation of a tropical depression (maximum sustained wind speed of 25 knots or more) was considered TC genesis. We also use the daily gridded SST data obtained from the National Oceanic and Atmospheric Administration Optimum Interpolation Sea Surface Temperature (OISST) version 2⁴⁴ with a spatial resolution 0.25° to detect MHW events. The atmospheric variables, including winds, specific humidity and latent heat fluxes were obtained from the European Centre for Medium-Range Weather Forecasts ERA5 reanalysis⁴⁵ with a spatial resolution 0.25° . To understand the related change in TCs, we use precipitation data from TRMM (TMPA) Level 3 Version 7 data with a horizontal resolution of 0.25° and temporal resolution of 3 hours, available only from 1998 to 2019. In analysis, we composited the precipitation into a daily time scale to remove the diurnal fluctuations in TC rainfalls⁴⁶.

Definition of MHW TC and non-MHW TC. The current study mainly focuses on comparing MHW TCs and non-MHW TCs to assess the impact of MHWs on TC intensification. For the classification into two groups, we first detected the MHWs following

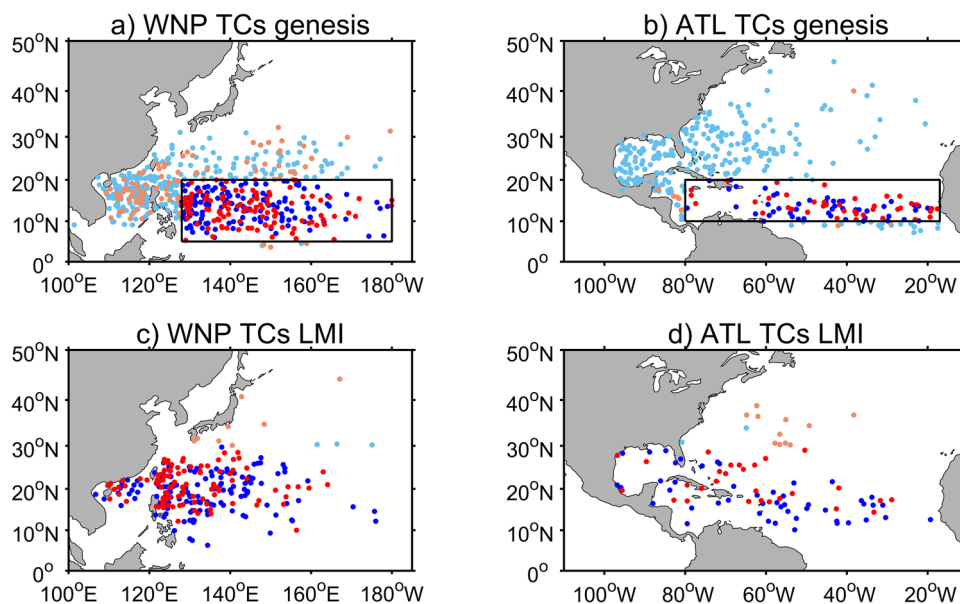


Fig. 5 The genesis and LMI locations of the MHW and non-MHW TCs. **a, c** show the WNP TC cases and **b, d** show the ATL TC. The dots colored red and blue denote the MHW and non-MHW TCs, respectively, and the faint colored dots denote the TCs excluded in this study. The black box line indicates the main development region.

Hobday et al.⁴⁷. MHW events are defined as periods when the daily SST exceeds a seasonally varying 90th percentile for a minimum of five consecutive days. The daily climatology of the 90th percentile was calculated based on the early 30-year period (1982–2011) by smoothing with an 11-day window centered on each day of the year. MHW duration is the length of the start to end date, intensity is the temperature anomaly above the climatology, and we count events in a particular period to define the frequency (Supplementary Fig. 5).

To examine the impact of an MHW on a TC in the intensification phase, we defined an MHW TC as a TC whose center stayed within 1 degree of an MHW area for two days or more before reaching the LMI. TCs that never encountered MHWs in their lifetime were defined as non-MHW TCs. This spatial threshold (1 degree of an MHW area) can cover the TC core area, so it can directly impact TC and the time threshold (more than 2 days) is enough time for impact on the TCs^{15,16}. Additionally, TCs that encountered an MHW region <24 hours before reaching the LMI or TCs that passed an MHW region after the LMI were excluded from this study. Examples of MHW TCs and non-MHW TCs are illustrated in Supplementary Figure 6. We also applied the geographical limitation on TC formation because the distribution of MHW and non-MHW TCs is unbalanced (Fig. 5a, b). Most MHW TCs formed over the southeastern area of the basin. The TCs that developed over this area could be more intense because they traveled over warm tropical oceans longer⁴⁸. To focus on the effect of MHWs and remove the possible influences from the formation location, we consider only the TCs that formed over the main development regions where about 79% of all major TC develop of the MHW TCs, which are marked as the box region of 128°–180°W, 5°–20°N for WNP (Fig. 5a) and 80°–15°W, 10°–20°N for ATL (Fig. 5b). Secondly, the latitude of the LMI was limited (Fig. 5c, d) under the 30°N because LMI latitude also affect the TC intensity^{49,50}. As a result, we defined a total of 128 MHW TCs and 184 non-MHW TCs, including 100 MHW TCs and 137 non-MHW TCs in the WNP and 28 MHW TCs and 47 non-MHW TCs in the ATL. All MHW TCs in this study have experienced the MHW more than two days in the last five days before LMI.

Data availability

NOAA 1/4° daily Optimum Interpolation Sea Surface Temperature is available from <https://psl.noaa.gov/data/gridded/data.noaa.oisst.v2.highres.html>. TC best track data are from the Joint Typhoon Warning Center (<https://www.metoc.navy.mil/jtwc/jtwc.html?best-tracks>) and Best Track data and the hurricane database (<https://www.nhc.noaa.gov/data/>). We obtained daily total precipitation from the TRMM(TMPA) Rainfall Estimate L3 V7 from https://disc.gsfc.nasa.gov/datasets/TRMM_3B42_7/summary. Atmospheric variables, including the latent heat flux, specific humidity, relative humidity, horizontal wind, and vertical velocity, are from the ECMWF Reanalysis version 5 (<https://cds.climate.copernicus.eu/cdsapp#!/dataset/reanalysis-era5-complete?tab=form>). Daily vertical ocean temperature data are from the GLORYS (<https://data.marine.copernicus.eu/products>). The data used to create the figures can be found at <https://github.com/h-ychoi/MHW-TC>.

Code availability

Codes used to generate main figures are available on request from the authors.

Received: 20 July 2023; Accepted: 24 January 2024;

Published online: 07 February 2024

References

1. Frölicher, T. L. & Laufkötter, C. Emerging risks from marine heat waves. *Nat. Commun.* **9**, 650 (2018).

2. Feng, M., McPhaden, M. J., Xie, S.-P. & Hafner, J. La Niña forces unprecedented Leeuwin Current warming in 2011. *Sci. Rep.* **3**, 1277 (2013).
3. Pearce, A. F. & Feng, M. The rise and fall of the “marine heat wave” off Western Australia during the summer of 2010/2011. *J. Mar. Syst.* **111–112**, 139–156 (2013).
4. Oliver, E. C. J. et al. The unprecedented 2015/16 Tasman Sea marine heatwave. *Nat. Commun.* **8**, 16101 (2017).
5. Lee, S., Park, M.-S., Kwon, M., Kim, Y. H. & Park, Y.-G. Two major modes of East Asian marine heatwaves. *Environ. Res. Lett.* **15**, 74008 (2020).
6. Olita, A. et al. Effects of the 2003 European heatwave on the Central Mediterranean Sea: surface fluxes and the dynamical response. *Ocean Sci.* **3**, 273–289 (2007).
7. Dzwonkowski, B. et al. Compounding impact of severe weather events fuels marine heatwave in the coastal ocean. *Nat. Commun.* **11**, 4623 (2020).
8. Oliver, E. C. J. et al. Longer and more frequent marine heatwaves over the past century. *Nat. Commun.* **9**, 1324 (2018).
9. Lee, S. et al. Rapidly changing East Asian marine heatwaves under a warming climate. *J. Geophys. Res. Ocean* **128**, e2023JC019761 (2023).
10. Elsner, J. B., Kossin, J. P. & Jagger, T. H. The increasing intensity of the strongest tropical cyclones. *Nature* **455**, 92–95 (2008).
11. Bender, M. A. et al. Modeled impact of anthropogenic warming on the frequency of intense Atlantic hurricanes. *Science* **327**, 454–458 (2010).
12. Kim, H.-S. et al. Tropical cyclone simulation and response to CO2 doubling in the GFDL CM2.5 high-resolution coupled climate model. *J. Clim.* **27**, 8034–8054 (2014).
13. Bengtsson, L. et al. How may tropical cyclones change in a warmer climate? *Tellus A: Dyn. Meteorol. Oceanogr.* **59**, 539–561 (2007).
14. Knutson, T. R. et al. Tropical cyclones and climate change. *Nat. Geosci.* **3**, 157–163 (2010).
15. Shay, L. K., Goni, G. J. & Black, P. G. Effects of a Warm Oceanic Feature on Hurricane Opal. *Mon. Weather Rev.* **128**, 1366–1383 (2000).
16. Lin, I.-I. et al. The interaction of super typhoon Maemi (2003) with a Warm Ocean Eddy. *Mon. Weather Rev.* **133**, 2635–2649 (2005).
17. Lin, I.-I., Pun, I.-F. & Lien, C.-C. “Category-6” super typhoon Haiyan in global warming hiatus: contribution from subsurface ocean warming. *Geophys. Res. Lett.* **41**, 8547–8553 (2014).
18. Huang, P., Lin, I.-I., Chou, C. & Huang, R.-H. Change in ocean subsurface environment to suppress tropical cyclone intensification under global warming. *Nat. Commun.* **6**, 7188 (2015).
19. Kataoka, T., Tozuka, T. & Yamagata, T. Generation and decay mechanisms of Ningaloo Niño/Niña. *J. Geophys. Res. Ocean.* **122**, 8913–8932 (2017).
20. Sen Gupta, A. et al. Drivers and impacts of the most extreme marine heatwave events. *Sci. Rep.* **10**, 19359 (2020).
21. Holbrook, N. J. et al. A global assessment of marine heatwaves and their drivers. *Nat. Commun.* **10**, 2624 (2019).
22. Rathore, S. et al. Interactions between a marine heatwave and tropical cyclone amphan in the Bay of Bengal in 2020. *Front. Clim.* **4**, 861477 (2022).
23. Chang, M., Ho, C.-H., Park, M.-S., Kim, J. & Ahn, M.-H. Multiday evolution of convective bursts during western North Pacific tropical cyclone development and nondevelopment using geostationary satellite measurements. *J. Geophys. Res. Atmos.* **122**, 1635–1649 (2017).
24. Park, D.-S. R., Ho, C.-H., Kim, J.-H. & Kim, H.-S. Spatially inhomogeneous trends of tropical cyclone intensity over the Western North Pacific for 1977–2010. *J. Clim.* **26**, 5088–5101 (2013).
25. Park, M.-S., Penny, A. B., Elsberry, R. L., Billings, B. J. & Doyle, J. D. Latent heating and cooling rates in developing and nondeveloping tropical disturbances during TCS-08: radar-equivalent retrievals from mesoscale numerical models and ELDORA. *J. Atmos. Sci.* **70**, 37–55 (2013).
26. Park, M.-S. et al. Land-based convection effects on formation of tropical cyclone Mekkhala (2008). *Mon. Weather Rev.* **145**, 1315–1337 (2017).
27. Hendricks, E. A., Montgomery, M. T. & Davis, C. A. The role of “vortical” hot towers in the formation of tropical cyclone Diana (1984). *J. Atmos. Sci.* **61**, 1209–1232 (2004).
28. Montgomery, M. T., Vladimirov, V. A. & Denissenko, P. V. An experimental study on hurricane mesovortices. *J. Fluid Mech.* **471**, 1–32 (2002).
29. Fritz, C., Wang, Z., Nesbitt, S. W. & Dunkerton, T. J. Vertical structure and contribution of different types of precipitation during Atlantic tropical cyclone formation as revealed by TRMM PR. *Geophys. Res. Lett.* **43**, 894–901 (2016).
30. Molinari, J. & Vollaro, D. Rapid intensification of a sheared tropical storm. *Mon. Weather Rev.* **138**, 3869–3885 (2010).
31. ECMWF. I. F. S. Documentation CY41R2 - part IV: physical processes. *IFS Documentation CY41R2* <https://doi.org/10.21957/tr5rv27xu> (2016).
32. Jaimes, B., Shay, L. K. & Brewster, J. K. Observed air-sea interactions in tropical cyclone Isaac over Loop Current mesoscale eddy features. *Dyn. Atmos. Ocean.* **76**, 306–324 (2016).
33. Jangir, B., Swain, D. & Ghose, S. K. Influence of eddies and tropical cyclone heat potential on intensity changes of tropical cyclones in the North Indian Ocean. *Adv. Space Res.* **68**, 773–786 (2021).

34. Gao, S. & Chiu, L. S. Surface latent heat flux and rainfall associated with rapidly intensifying tropical cyclones over the western North Pacific. *Int. J. Remote Sens.* **31**, 4699–4710 (2010).
35. Gao, S., Zhai, S., Chiu, L. S. & Xia, D. Satellite air–sea enthalpy flux and intensity change of tropical cyclones over the western North Pacific. *J. Appl. Meteorol. Climatol.* **55**, 425–444 (2016).
36. Jaimes, B., Shay, L. K. & Uhlhorn, E. W. Enthalpy and momentum fluxes during hurricane earl relative to underlying ocean features. *Mon. Weather Rev.* **143**, 111–131 (2015).
37. Lin, I.-I., Wu, C.-C., Pun, I.-F. & Ko, D.-S. Upper-ocean thermal structure and the western north pacific category 5 typhoons. Part I: ocean features and the category 5 typhoons’ intensification. *Mon. Weather Rev.* **136**, 3288–3306 (2008).
38. Raymond, D. J., Sessions, S. L. & López Carrillo, C. Thermodynamics of tropical cyclogenesis in the northwest Pacific. *J. Geophys. Res. Atmos.* **116**, D18101 (2011).
39. Park, M.-S. & Elsberry, R. L. Latent heating and cooling rates in developing and nondeveloping tropical disturbances during TCS-08: TRMM PR versus ELDORA retrievals. *J. Atmos. Sci.* **70**, 15–35 (2013).
40. Fritz, C. & Wang, Z. Water vapor budget in a developing tropical cyclone and its implication for tropical cyclone formation. *J. Atmos. Sci.* **71**, 4321–4332 (2014).
41. Park, M.-S., Elsberry, R. L. & Harr, P. A. Vertical wind shear and ocean heat content as environmental modulators of western north pacific tropical cyclone intensification and decay. *Trop. Cyclone Res. Rev.* **1**, 448–457 (2012).
42. Plecha, S. M. & Soares, P. M. M. Global marine heatwave events using the new CMIP6 multi-model ensemble: from shortcomings in present climate to future projections. *Environ. Res. Lett.* **15**, 124058 (2020).
43. Park, M.-S. et al. Regional cloud characteristics over the tropical northwestern Pacific as revealed by Tropical Rainfall Measuring Mission (TRMM) Precipitation Radar and TRMM Microwave Imager. *J. Geophys. Res. Atmos.* **112**, D05209 (2007).
44. Huang, B. et al. Improvements of the daily optimum interpolation sea surface temperature (DOISST) version 2.1. *J. Clim.* **34**, 2923–2939 (2021).
45. Hersbach, H. et al. The ERA5 global reanalysis. *Q. J. R. Meteorol. Soc.* **146**, 1999–2049 (2020).
46. Bowman, K. P. & Fowler, M. D. The diurnal cycle of precipitation in tropical cyclones. *J. Clim.* **28**, 5325–5334 (2015).
47. Hobday, A. J. et al. A hierarchical approach to defining marine heatwaves. *Prog. Oceanogr.* **141**, 227–238 (2016).
48. Daloz, A. S. & Camargo, S. J. Is the poleward migration of tropical cyclone maximum intensity associated with a poleward migration of tropical cyclone genesis? *Clim. Dyn.* **50**, 705–715 (2018).
49. Moon, I.-J., Kim, S.-H., Klotzbach, P. & Chan, J. C. L. Roles of interbasin frequency changes in the poleward shifts of the maximum intensity location of tropical cyclones. *Environ. Res. Lett.* **10**, 104004 (2015).
50. Kim, H.-S., Park, D.-S. R., Ho, C.-H., Moon, I.-J. & Chan, J. C. L. Latitudinal variation of the lifetime maximum intensity location of atlantic tropical cyclones controlled by the atlantic multidecadal oscillation. *Geophys. Res. Lett.* **49**, e2021GL097459 (2022).

Acknowledgements

This research was supported by the National Research Foundation of Korea (NRF) grant funded by the Korean government (MSIT) (2021R1A2C1014608 and RS-2023-00207866). This study was also supported by the Korea Institute of Marine Science and Technology Promotion (KIMST), funded by the Ministry of Oceans and Fisheries (20220566).

Author contributions

Conceptualization: Myung-Sook Park and Hyeog-Seog Kim. Methodology: Hwan-Young Choi, Hyeog-Seog Kim, and Seonju Lee. Investigation: Hwan-Young Choi, Myung-Sook Park, Hyeog-Seog Kim, and Seonju Lee. Visualization: Hwan-Young Choi. Funding acquisition: Myung-Sook Park and Hyeog-Seog Kim. Supervision: Myung-Sook Park and Hyeog-Seog Kim. Writing—original draft: Hwan-Young Choi. Writing—review & editing: Myung-Sook Park and Hyeog-Seog Kim.

Competing interests

The authors declare no competing interests.

Additional information

Supplementary information The online version contains supplementary material available at <https://doi.org/10.1038/s43247-024-01239-4>.

Correspondence and requests for materials should be addressed to Myung-Sook Park or Hyeog-Seog Kim.

Peer review information *Communications Earth & Environment* thanks Vineet Kumar Singh and the other, anonymous, reviewer(s) for their contribution to the peer review of this work. Primary Handling Editors: Heike Langenberg, Aliénor Lavergne. A peer review file is available.

Reprints and permission information is available at <http://www.nature.com/reprints>

Publisher’s note Springer Nature remains neutral with regard to jurisdictional claims in published maps and institutional affiliations.



Open Access This article is licensed under a Creative Commons Attribution 4.0 International License, which permits use, sharing, adaptation, distribution and reproduction in any medium or format, as long as you give appropriate credit to the original author(s) and the source, provide a link to the Creative Commons license, and indicate if changes were made. The images or other third party material in this article are included in the article’s Creative Commons license, unless indicated otherwise in a credit line to the material. If material is not included in the article’s Creative Commons license and your intended use is not permitted by statutory regulation or exceeds the permitted use, you will need to obtain permission directly from the copyright holder. To view a copy of this license, visit <http://creativecommons.org/licenses/by/4.0/>.

© The Author(s) 2024